Arabian Journal of Chemistry (2022) **15**, 103606

King Saud University

Arabian Journal of Chemistry

www.ksu.edu.sa
www.sciencedirect.com

ORIGINAL ARTICLE

A novel approach for fabrication ZnO/CuO nanocomposite via laser ablation in liquid and its antibacterial activity

Abbad Al Baroot [a,b,*], Muidh Alheshibri [c,b], Q.A. Drmosh [d], Sultan Akhtar [e], Essam Kotb [f,b], Khaled A. Elsayed [a]

[a] *Department of Basic Engineering Sciences, College of Engineering, Imam Abdulrahman Bin Faisal University, P.O. Box 1982, Dammam 31441, Saudi Arabia*
[b] *Basic & Applied Scientific Research Centre, Imam Abdulrahman Bin Faisal University, P.O. Box 1982, Dammam 31441, Saudi Arabia*
[c] *Department of Basic Sciences, Deanship of Preparatory Year and Supporting Studies, Imam Abdulrahman Bin Faisal University, P.O. Box 1982, Dammam 31441, Saudi Arabia*
[d] *Interdisciplinary Research Center for Hydrogen and Energy Storage (IRC-HES), King Fahd University of Petroleum and Minerals (KFUPM), Dhahran 31261, Saudi Arabia*
[e] *Department of Biophysics, Institute for Research and Medical Consultations (IRMC), Imam Abdulrahman Bin Faisal University, P.O. Box 1982, Dammam 31441, Saudi Arabia*
[f] *Department of Biology, College of Science, Imam Abdulrahman Bin Faisal University, Dammam, Saudi Arabia*

Received 11 October 2021; accepted 2 December 2021
Available online 09 December 2021

KEYWORDS

Hetrostructure nanocomposits;
Pulsed laser ablation;
Spray pyrolysis;
Antibacterial activity;
Zinc Oxide-Copper Oxide

Abstract Pulsed laser ablation in liquid (PLAL) has verified its surpassing advantages in the fabrication of several high purity nanostructured metals and metal oxides. In this work, ZnO/CuO heterostructure nanocomposites have been fabricated by laser ablation a Q switched Nd: YAG laser beam (1064 nm, 10 Hz, pulse energy and pulse with 30 mJ and 10 ns) is focused on the surface of the ZnO thin film for 10 min. The fabricated ZnO/CuO nanocomposite was then characterized using transmission electron microscopy (TEM), UV–vis spectrophotometer, X-ray diffraction (XRD), and Raman spectroscopy to investigate the structural, compositional, and optical properties of the fabricated nanocomposite. The synthesized nanocomposites were evaluated as antibacterial agents against both the gram-positive bacterium *S. aureus* subsp. aureus ATCCBAA-977, and the gram-negative bacteria *E. coli* ATCC8739, *K. pneumoniae* subsp. pneumoniae ATCC700603, and *P. aeruginosa* ATCC27853. The as-fabricated ZnO/CuO nanocomposite demonstrated

* Corresponding author.
E-mail address: afalbaroo@iau.edu.sa (A. Al Baroot).
Peer review under responsibility of King Saud University.

Production and hosting by Elsevier

https://doi.org/10.1016/j.arabjc.2021.103606

outstanding antibacterial activity except in the case of *K. pneumoniae* subsp. pneumoniae ATCC700603 while the maximum activity was observed against *E. coli* ATCC8739.

1. Introduction

Heterostructure nanocomposites (HNCs) have a wide range of applications in photocatalysis (Iqbal et al., 2021), hydrogen production (Enesca and Andronic, 2021), organic pollutant removal (Enesca and Andronic, 2021), electrochemical sensor (Kokulnathan et al., 2021), and antibacterial activity (Kokilavani et al., 2021). Further, they are one of the greatest practical interest topics that have been studied by the scientific community recently (Iqbal et al., 2021; Sumesh, 2020; Wang et al., 2020; Salehi-Babarsad et al., 2020; Hermawan et al., 2020; Draz et al., 2021; Biswal et al., 2021). HNCs can be fabricated by a combination of two or more materials such as metal oxide/metal oxide, metal sulfide/metal oxide, etc. (Mendonça et al., 2021). These combinations of two or more materials lead to produce heterostructure nanocomposites with unique properties that differ from the properties of individual compounds. One of several methods have used to synthesize nanocomposite; is a top-down technique. Top-down techniques such as laser ablation, ball mailing, and sputtering are based on disassembling the bulk target/powder into small pieces, (Zarschler et al., 2016; Giner-Casares et al., 2016; Mendonça et al., 2021). These methods allow rapid, simple, versatile, low-cost and automated synthesis compared to many other techniques. Laser ablation of solid metal targets in aqueous media has been extensively utilized to fabricate several heterostructure nanocomposites. (Mendonça et al., 2021; Zhang et al., 2020) . The technique is quite attractive for researchers due to its ability to fabricate high-quality nanoparticles that have various advantages over the other methods. (Dhongade et al., 2020) Mostafa *et al.* fabricated Au/SnO_2 nanocomposite for antibacterial activity against two different bacteria. This investigation reported their efficient antibacterial activity against *E. coli* compared to *Bacillus subtilis*. (Mostafa and Mwafy, 2020) Menazea et al. recently synthesized TiO_2/ZnO nanocomposites using pulsed laser ablation and studied their antibacterial activity. The activity index of the antibacterial activity was shown to be enhanced in the TiO_2/ZnO compared to its individual (Menazea, 2020).

Alswat et al. reported that both CuO and ZnO at a low concentration are very safe for human cells as well as non-toxic material, which leads them to be suitable additives for materials that are used as antibacterial agents; Further, both of them have significant biological applications and demonstrated a broad range of antibacterial activities for various microorganisms,. (Mostafa and Mwafy, 2020; Rishikesan and Basha, 2020; Alswat et al., 2017; Ahamed et al., 2014; Mwafy et al., 2019; Mostafa et al., 2020; Mostafa and Mwafy, 2020) Recently, Merugu et al. evaluated Cu- doped ZnO nanoparticles against two gram-positive bacterial strains (Bacillus subtilis and Staphylococcus aureus) and two gram-negative bacterial strains (Pseudomonas aeruginosa and Escherichia coli). The antibacterial activity was only observed against gram-positive bacteria (Khan et al., 2020). Furthermore, Liu et al. showed that CuO/ZnO nanocomposites have superior antibacterial activity than their individual components (Das and Srivastava, 2018). Fabrication of nanocomposites using pulsed laser ablation of different targets is time-consuming. To overcome this issue, laser ablation of a deposited thin film with different composites on a metal target is expected to facilitate the formation of nanocomposites and reduce the time needed to fabricate such nanocomposites. We are not aware of any work that has considered fabricating nanocomposites using deposited thin films on metal targets for antibacterials studies. Furthermore, spray pyrolysis is one of the most straightforward techniques that have been used to deposit thin film with many benefits, i.e. low cost, easy to use, coat over the large area and inexpensive instrument compared with other instruments (Grosso et al., 2015; Perednis and Gauckler, 2005; Filipovic et al., 2014).

The goal of this work is to synthesize zinc oxide/copper oxide (ZnO/CuO) nanocomposite by pulsed laser ablation of ZnO thin films deposited into Cu target in water and investigate them as antibacterial agents against both the gram-positive bacterium *S. aureus* subsp. aureus ATCCBAA-977, and the gram-negative bacteria *E. coli* ATCC8739, *K. pneumoniae* subsp. pneumoniae ATCC700603, and *P. aeruginosa* ATCC27853. The fabricated ZnO/CuO nanocomposite was characterized using transmission electron microscopy (TEM), UV–vis spectrophotometer, X-ray diffraction (XRD) and Raman spectroscopy to investigate the structural, compositional, and optical properties of the fabricated nanocomposite.

2. Experimental section

The steps involved in the fabrication of ZnO/CuO nanocomposite are shown in Fig. 1. In general, the fabrication steps are divided into two main steps as follows.

2.1. Preparation of ZnO thin films on a copper target

A thin layer of ZnO was deposited into a metallic copper using spray pyrolysis. The method used to fabricate ZnO thin film in this work is similar to that reported by Lehraki *et al.* (Yan et al., 2010) and Bacaksiz *et al.* (Bacaksiz et al., 2008). After applying the traditional cleaning procedures, 100 mM of zinc chloride was used as the optimum molarity to synthesize highly crystalline ZnO film. It is well established that high crystallinity is the most common advantage of this optimum molarity (Raj Mohamed and Amalraj, 2016). Deionized water was used to dissolve the salt of a zinc chloride; when the solution dissolved very well, we can spray that solution onto a substrate that was held at temperatures 400 °C on a hot plate by using a pressure air atomizer at 1.5 bar pressure. In particular, a commercial GaGa Milano 134 K airbrush with a 0.2 mm

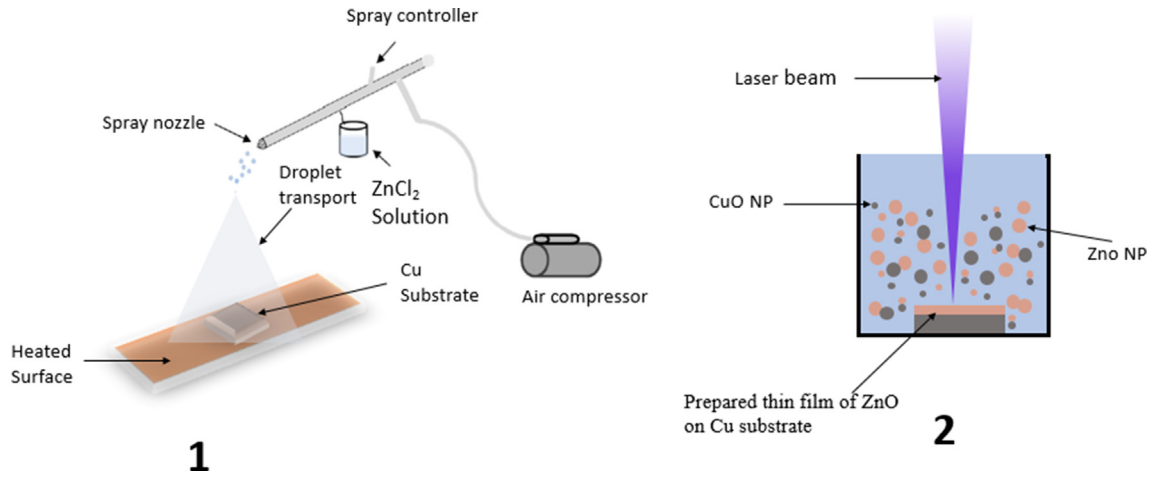

Fig. 1 The schematic set-up consists of two steps (1) ZnO thin films deposited by spray pyrolysis on copper solid metal targe (2) laser ablation process in aqueous solution.

nozzle was used to prepare thin films of our samples. The detailed spraying technique of metal chloride to convert to ZnO has been reported in recent work. (Althagafi et al., 2016; Al Baroot and Grell, 2019) Briefly, the mechanism of conversion from ZnCl2 to ZnO by spray pyrolysis has been described by Falcony et al. (Falcony et al., 2018). They have described the mechanism by four steps which happen when the droplet is exposed to different surface temperatures in two scenarios. Here, we have considered an extremely high temperature of 400C of Cu metal target on the hot plate; in this case, the size of the droplet is tiny; within the vapour phase, the vaporized precipitate is subjected to a chemical reaction and turned to the powder prior to reaching the surface of the copper substrate. In this work, 12 layers of ZnO were deposited on Cu metal target, with the thickness of 260 ± 10 nm measured by Dektak profilometer as reported in our previous work (Althagafi et al., 2016).

2.2. Synthesis of ZnO/CuO nanocomposite

In this step, as-prepared ZnO thin film was put at the bottom of the glass vail filled with 7 mL of double-distilled water. The height of the water level above the thin film was about 1 cm. A Q switched Nd: YAG laser beam (1064 nm, 10 Hz, pulse energy and pulse with 30 mJ and 10 ns) was focused on the surface of the thin film by a 10 cm bi-convex lens. The spot size on the surface of the thin film was adjusted by the distance between the thin film sample and the bi-convex lens. The spot size was 1 mm, and hence the laser fluence was 3.8 J/cm^2. The focused laser beam was scanned on the surface of the sample manually to avoid the formation of any crater and to ablate both ZnO thin films along with the pure Cu substrate. The laser ablation process lasted for 10 min. During the laser ablation, a magnetic stir was used to remove the freshly formed nano collide from the path of the laser beam as more detailed reported in recent work (Alheshibri et al., 2021; Elsayed et al., 2021).

The ZnO/CuO nanocomposite should be stored in a well-cleaned flask to perform several characterizations on the samples. The sample has been then characterized by XRD, Raman, Uv.vis spectrophotometer and a TEM).

2.3. Characterization techniques

The phase identification and structure of the fabricated samples were investigated via the diffractometer Shimadzu-6000, operating at 40 mA, 30 kV, and 0.25°/min-scanning rate in the diffraction range between 2θ = 20° to 80°. Regarding the sample preparation for XRD, a few drops of as-fabricated materials were dropped onto an amorphous glass substrate and dried in Linkam stage at 110 ^{0}C for 20 min. The Raman spectra of the fabricated samples were recorded using DXR™3 Raman Microscope with laser energy of 10 mW and an excitation wavelength of 455 nm.

The optical properties of the ZnO/CuO nanocomposite were investigated in an aqueous solution using a UV–Vis spectrophotometer (Model SolidSpace-3700). Quartz cuvettes 10 mm were used to study the absorbance of CuO and ZnO/CuO nanocomposite. The Absorbance spectra were recorded between 200 and 900 nm. Further, the bandgap of ZnO/CuO nanocomposite was calculated.

The PLAL prepared CuO and ZnO/CuO composite specimens were analyzed by transmission electron microscopy (TEM) (FEI, Morgagni 268 at 80 kV). A droplet of each specimen dispersion was deposited onto the TEM grid having a holey carbon support film. The prepared grids were air-dried and mounted into the TEM. The TEM was performed at an accelerating voltage of 80 kV. Selected area electron diffraction (SAED) was also carried in TEM in order to clarify the crystalline structure and to highlight further the presence of ZnO particles in the composite product.

2.4. In-vitro antibacterial activity of the fabricated nanoparticles and the ZnO/CuO nanocomposite

Fabricated nanocomposite initial stock suspensions were prepared at a concentration of 50 µg/mL deionized water. The antibacterial activity of the fabricated samples was evaluated

by measuring the resulting inhibition zones (mm) in seeded Muller-Hington agar by a formerly adapted method of Beecher and Wong (Beecher and Wong, 1994), against selected clinical bacterial strains such as *E. coli* ATCC8739, *S. aureus* subsp. ATCCBAA-977, *P. aeruginosa* ATCC27853, and *K. pneumoniae* subsp. pneumoniae ATCC700603. The Müller–Hington agar consists of Beef extract (30%), Casein hydrolysate (1.75%), Starch (0.15%) and Agar (1.7%), autoclaved at 121 °C for 15 min then cooled to 47 °C and showed with the examined bacteria under aseptic conditions. After solidification, 5 mm diameter holes were pressed by a sterilized cork-borer. The examined NPs and HNC were then added into the holes at 50 µLvolume after being suspended in deionized water culture plates were then incubated for 18 h at 37 °C. The diameter of the inhibition zones in mm was measured to determine the antibacterial activity. All culture media were equipped following the producer's guidelines. Bacterial cultures were kept at 4 °C in HIA. The strains were subcultured, before the assessments, using the aforementioned media and incubated for 24 h at 37 °C. (Clinical, 2018; Palomino et al., 2002; Javadpour et al., 1996).

3. Results and discussion

Fig. 2 shows the XRD patterns of CuO and ZnO/CuO nanocomposites synthesized by the pulsed laser ablation in liquid. As can be seen, all of the peaks in the CuO sample could be indexed to the monoclinic structure of CuO (JCPDS # 89–2531), which is in good agreement with the previous studies. (Veisi et al., 2021; Tiwari and Shweta; Singh, A. K., Singh, V. P., Prasad, S. M., Ramawat, N., Tripathi, D. K., Chauhan, D. K., Rai, A. K. , 2019) The diffraction peaks located at 2θ = 31.79°; 34.47 °, 36.32°, 47.56°, 56.67°, 62.94°, 66.48°, 68.04°, 69.19°, 72.65°, and 77.04° can be perfectly indexed to (100), (002), (101), (102), (110), (103), (200), (112), (201), (004), and (202) of hexagonal ZnO; while the diffraction peaks observed at 2θ = 32.65°, 35.72°, 38.85°, 48.84°, 53.69°, 58.17°, 61.56°, 67.95°, and 75.35° are indexed to the (110), (002), (111), (−202), (020), (202), (−113), (113), and (–222) diffraction peaks of monoclinic CuO (JCPDS # 89–2531) suggesting the successful integration of the two compounds. (Rawat et al., 2019; Gondal et al., 2009) In addition, no other diffraction peaks were observed, confirming the high purity of the nanocomposite synthesized by pulsed laser ablation in liquid. The average particle sizes (APS) of CuO and ZnO were calculated using the Scherrer formula (Cullity, 1956):

$$APS = \frac{0.9\lambda}{FWHM cos\theta} \quad (1)$$

where λ is the wavelength of the XRD (Cu-$k_{\alpha 1}$ = 1.5406 Å), FWHM is the full width at half maximum. The average particle sizes of the CuO and ZnO nanoparticles in the ZnO/CuO nanocomposite were found to be 11 ± 1 and 25 ± 1 nm, respectively.

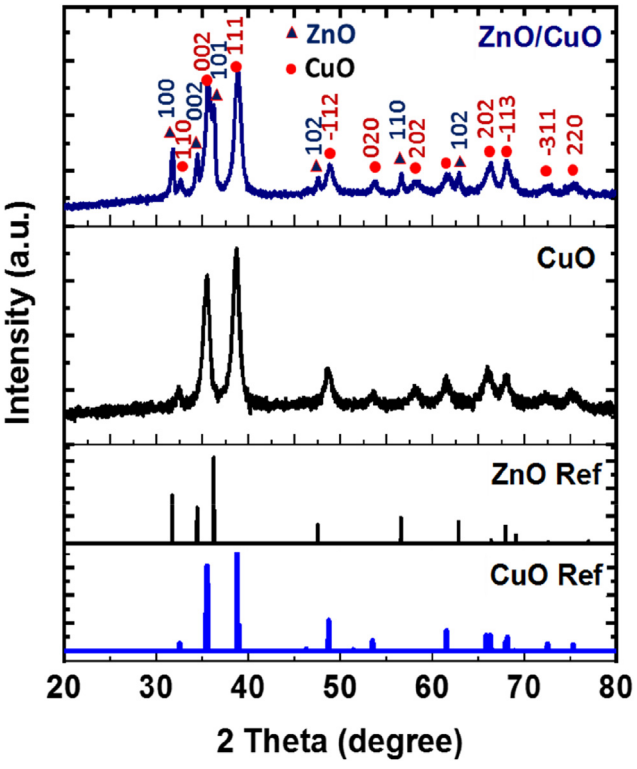

Fig. 2 XRD patterns of CuO nanoparticles, ZnO/CuO nanocomposite synthesized using pulsed laser ablation in liquid, and standard XRD patterns of ZnO and CuO.

The Raman spectra of the CuO and ZnO/CuO nanocomposite are recorded at room temperature and displayed in Fig. 3. Earlier reports have demonstrated that CuO nanoparticles with monoclinic structure and four atoms (two molecules) per unit cell belong to C_{2h}^6 and has twelve phonon branches (Joya et al., 2019). There are three acoustic modes with symmetries $A_g + 2B_g$ and nine zones centre optical modes with symmetries $4A_g + 5B_g$. Among the optical phonon modes, six modes ($3A_g + 3B_g$) are IR active, and the remaining three modes ($2B_g + A_g$) are Raman-active. (Hagemann et al., 1990; Prabhu et al., 2017; Bade B. R.; Rondiya S. R.; Hase Y. V.; Nasane M. P.; Jathar S. B.; Barma S. V.; Kore K. B.; Nilegave D. S.; Jadkar S. R.; Funde A. M, 2021) As can be seen, the Raman spectra of CuO nanoparticles prepared in this work are observed at 270.9, 321.7, and 603.8 cm^{-1} which can be assigned to A_g, B_g, and B_g, respectively. Comparing with the Raman spectrum of a single crystal CuO, the obtained Raman peaks are occurred downshift and have broadened, which could be ascribed to the quantum-size confinement effect of the fabricated CuO nanoparticles (Fang and Xuan, 2017). On the other hand, wurtzite ZnO belongs to the C_{6v}^4 with four atoms per unit cell, and group theory predicts that the optical phonons for ZnO can be expressed as A1 + 2B1 + E1 + 2E2 where the B1 modes are silent, and other modes (E1, E2, A1) are Raman active. Fig. 3 displays the Raman spectrum of the ZnO/CuO nanocomposite. Apparently, the Raman spectra of ZnO/CuO nanocomposite sample are observed at 205.4, 271.1, 321.2, 426.6, 591.6, 1120.1 cm^{-1}, which is a combination of both Raman spectra of CuO and ZnO nanoparticles, indicating the successful formation of the ZnO/CuO nanocomposite. There is no other obvious peak related to Cu_2O modes, which indicates that the ZnO/CuO

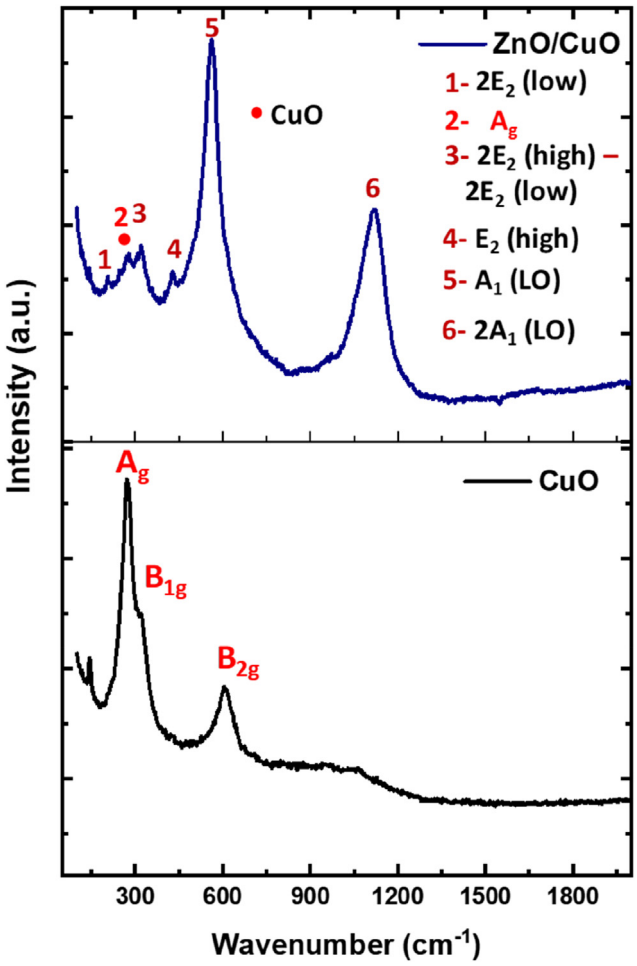

Fig. 3 Raman spectra of CuO and ZnO/CuO nanocomposite fabricated by pulsed laser ablation technique.

nanocomposite prepared by pulsed laser ablation in a liquid have only a single-phase property.

Absorption spectra and the corresponding band gaps of CuO nanoparticles and ZnO/CuO nanocomposite fabricated via pulsed laser ablation in liquid are presented in Fig. 4. ZnO nanomaterial results have been reported recently in our previous work with a report (Althagafi et al., 2016). For the case of the CuO nanoparticles and ZnO/CuO nanocomposite, both of them displayed the UV–Vis absorption characteristic, with a peak at 295 nm and a minor peak at 360 nm, related to the material of CuO (Fig. 4).. Further, From the absorption data, Tauc plots are analyzed to determine the bandgap energies of the product materials synthesized CuO nanoparticles and ZnO/CuO nanocomposite. They can be found by this well-known equation.

$$(\alpha h\nu)^n = B\left(h\nu - E_g\right) \quad (2)$$

where $h\nu$ is the photo energy, B is a constant correlated to the specific material, α is the coefficient of absorption, and n can be 2 for a direct transition or can be 1/2 for an indirect transition. As it is obvious from the Tauc plots that the bandgap energy of CuO nanoparticles is about 2.1 eV . The obtained optical bandgap is slightly higher than that of bulk CuO (1.8 eV), which could be ascribed to the confinement effect. (Das et al., 2018; Han et al., 2019) The quantum confinement proposes that holes and electrons in the nanostructured semiconductor, especially nano-sized materials having a grain size less than 20 nm, are confined by the potential barriers of the surface or by a potential well of the quantum box, which involves the increase of the bandgap between the conduction band and the valance band (Daira et al., 2020). The bandgap of ZnO/CuO nanocomposite is found to be 2.6 eV. This value is lower than that of ZnO (3.37 eV) and could be attributed to the existence of CuO impurities in the ZnO structure.

Fig. 5 shows the TEM images and SAED patterns for pure CuO nanoparticles and ZnO/CuO composite specimens prepared by the PLAL method. The CuO specimen shows the spherical shaped particles with a wide size distribution. The size of particles is a small as 5 nm and as large as 80 nm. The maximum number of particles were found between the size range of 5–20 nm. It was observed that the particles were interlinked and showed a network-like morphology. The SAED pattern displayed the continuous rings and was well separated to each, suggesting the polycrystalline nature of the particles. The SAED pattern was identical to CuO nanoparticles, where the rings were labelled as (started from the inner ring): (1 1 0), (0 0 2), (1 1 1), (2 0 2), (0 2 0) and (0 2 2), verified by the pdf JCPDS file No.45–0937 for the monoclinic crystal (a = 0.46 853 nm, b = 0.34257 nm and c = 0.51303 nm) (Dey et al., 2012). The ZnO/CuO composite specimen showed the particles of both CuO and ZnO as confirmed by the varied morphology as observed in the case of individual CuO specimen. The presence of the ZnO in the CuO was further confirmed by the SAED pattern. The SAED pattern of ZnO/CuO displayed the additional rings or dotted rings for ZnO, a combination pattern of ZnO and CuO. The additional rings, as compared to CuO are appeared within the previously indicated rings of CuO as highlighted by yellow dotted circles. The ZnO intensities are indexed as (1 0 0), (0 0 2) and (1 0 1) additional to CuO rings (Silambarasan et al., 2014). TEM and SAED results confirmed the successful synthesis of ZnO/CuO nanocomposite by applying the pulsed laser method in liquid.

To highlight the preparation of ZnO thin film and the exposure of ZnO/CuO substrate during the PLAL process, scanning electron microscopy (SEM) was performed on three substrates: pure copper and ZnO/CuO substrates before and after PLAL experiments. SEM micrographs of pure copper, ZnO/CuO substrate before PLAL experiment and ZnO/CuO substrate after PLAL experiment is shown in Fig. 6. Moreover, the digital photos of the three substrates were also shown as a top row (slab dimensions are $1 \times 1.5\ cm^2$). By digital photos, it was observed that the colour of the virgin copper was changed from light orange to purple after deposition, an indication of successful formation of ZnO thin film over copper. The ZnO/Cu substrate displayed an obvious laser-induced crater after PLAL experiment. From SEM, pure copper showed the striation lines and rough surface, a typical feature of the copper substrate (Ibrahim et al., 2015). The typical surface features were covered and diminished when deposited the thin film on copper where granular of ZnO particles can be seen resulting a comparatively smooth surface compared to pure

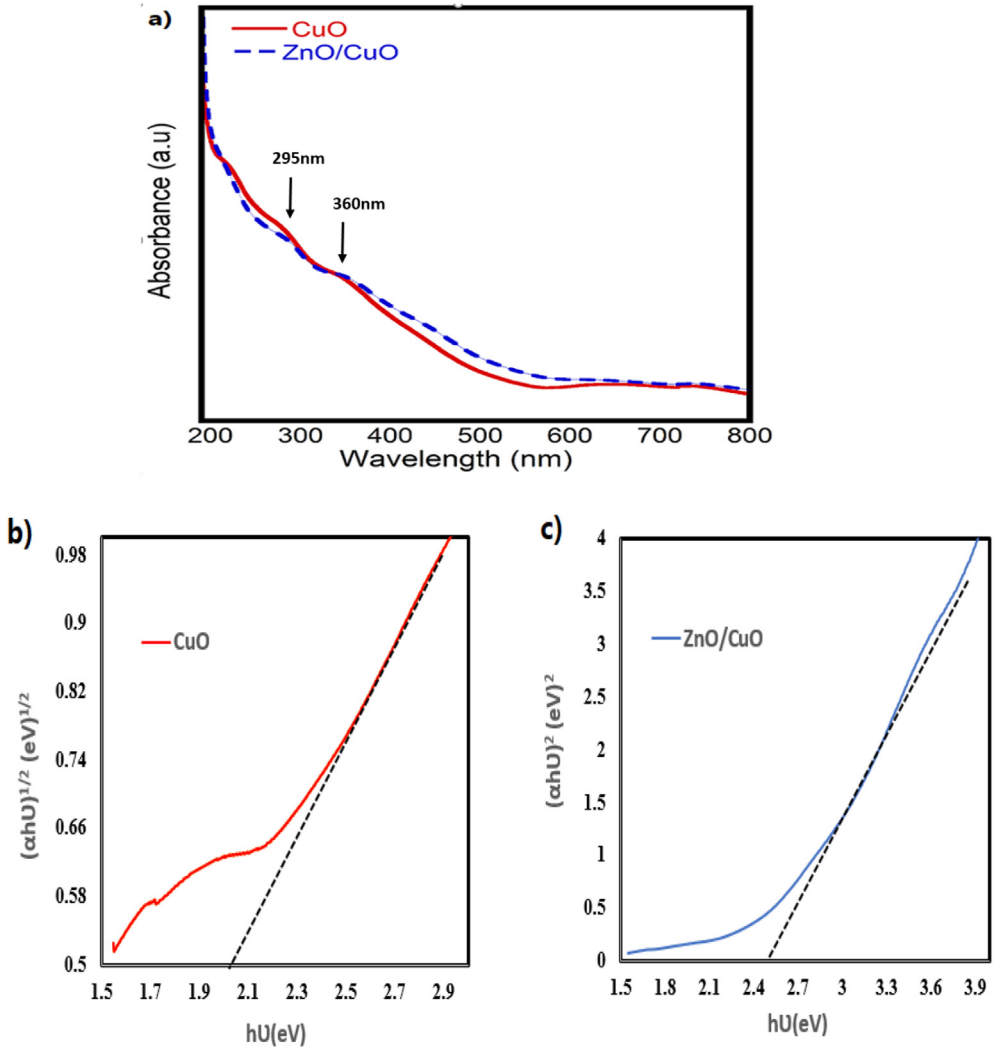

Fig. 4 (**a**) Absorption spectra of synthesized product material CuO and ZnO/CuO nanocomposite obtained at 10 min of ablation in the DI water. (**b**) the Tauc plot to find the band gap of CuO (**c**) and ZnO/CuO nanocomposite, respectively.

copper. Upon laser exposure during PLAL experiment, the morphology of the ZnO/CuO substrate was varied; it showed a network and laminar structure along with small/large holes and spherical/elongated particles.

4. Antibacterial studies

From Table 1, it appears that the CuO nanoparticles have antibacterial activity against both the gram-positive bacterium *S. aureus* subsp. aureus ATCCBAA-977 and the gram-negative bacteria *E. coli* ATCC8739, *K. pneumonia* subsp. pneumoniae, and *P. aeruginosa* ATCC27853. The combination of both CuO nanoparticles and ZnO nanoparticles have exerted superior activity except in the case of *K. pneumonia* subsp. pneumonia. The best antibacterial effect was noticed against *E. coli* ATCC8739 (Table 1 and Fig. 7). The least antibacterial activity of tested nanoparticles against the bacterium *Klebsiella pneumonia* subsp. Pneumonia may be attributed to the large mucoid capsule surrounding the cells.

In reference to other investigators, CuO and ZnO NPs have shown promising antibacterial activity when used alone and in nanocomposites (Allahyari et al., 2014; Saravanakkumar et al., 2018). The superior antibacterial activity of the nanocomposite against the bacterium *E. coli* in comparison with other tested bacteria agrees with the results of the ZnO/CuO nanocomposite prepared by Mohammadi-Aloucheh et al. using the green synthesis approach (Mohammadi-Aloucheh et al., 2018). While disagreeing with the results of Saravanakkumar and coworkers where *E. coli* in their study was the lowest sensitive bacterium among the tested bacteria to the nanocomposite prepared by a modified perfume chemical vapour deposition, i.e. spray pyrolysis technique (Saravanakkumar et al., 2018).

The antibacterial activity of ZnO/CuO nanocomposites may be due to (1) their capacity to hook up thiol groups (–SH groups) located on the bacterial cell membranes, leading to cell cracking and lysis (Li et al., 2015), (2) their ability to induce the production of high amounts of reactive oxygen species (Saravanakkumar et al., 2018), and (3) the release of Zn^{2+} from the nanocomposite tracked by the production of highly

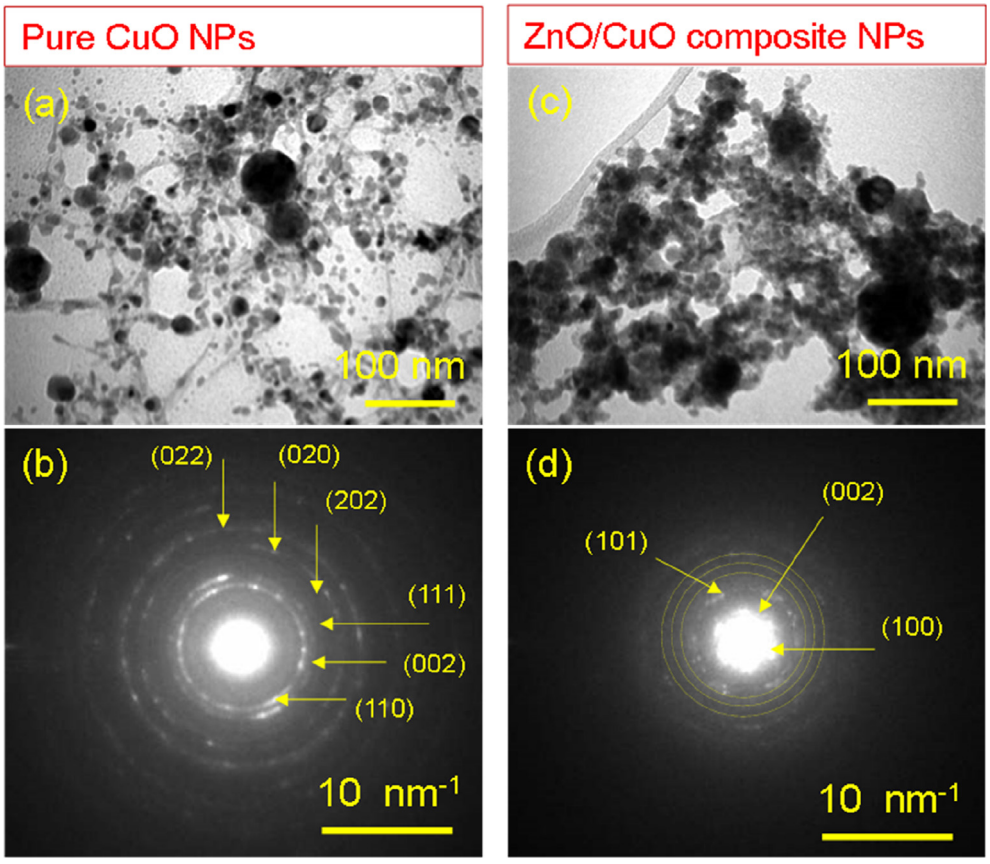

Fig. 5 (a, b) TEM image and corresponding SAED pattern of pure CuO NPs; (c, d) TEM image and corresponding SAED pattern of ZnO/CuO nanocomposite.

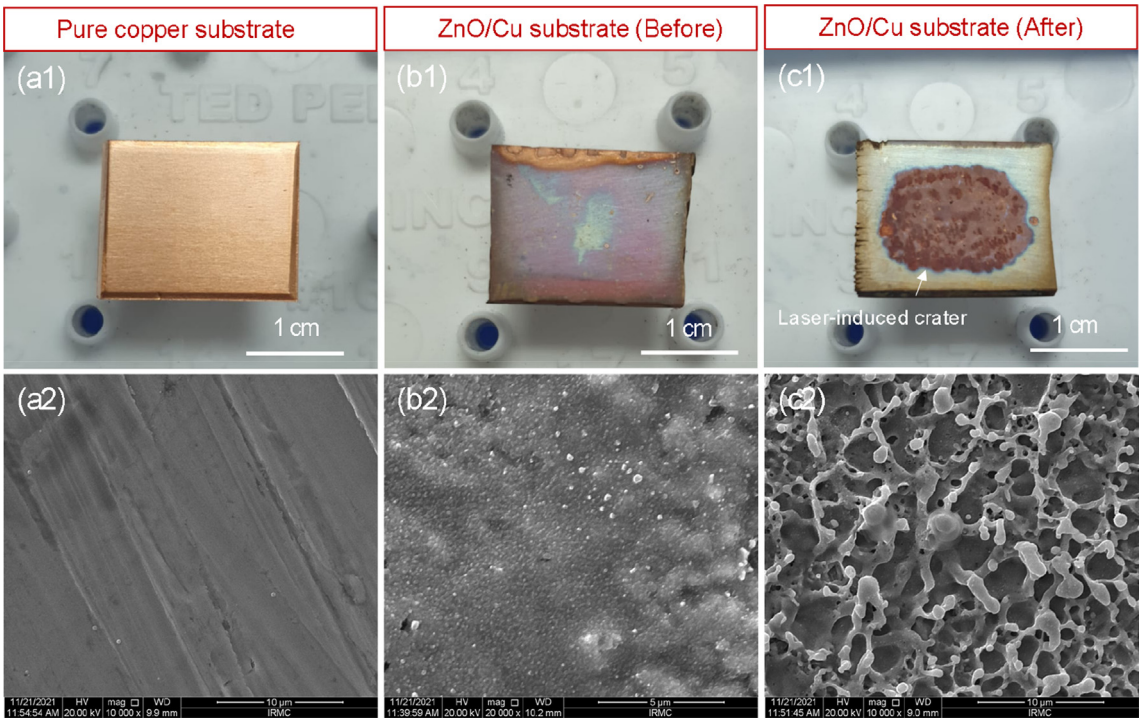

Fig. 6 Digital photos and SEM micrographs of (a1, a2) pure copper, ZnO/Cu substrate (b1, b2) before and after (c1, c2) PLAL experiment.

Table 1 The antibacterial activity of the newly prepared nanoparticle and nanocomposite.

Tested bacterium	Antibacterial activity (mm)	
	Pure CuO NPs	*ZnO/CuO nanocomposite*
E. coli ATCC8739	16.5 ± 0.2	24.0 ± 1.6
K. pneumonia subsp. pneumonia	9.5 ± 0.4	0.0 ± 0.0
P. aeruginosa ATCC27853	12.0 ± 0.5	13.0 ± 0.6
S. aureus subsp. aureus ATCCBAA-977	14.5 ± 1.2	18.5 ± 1.0

reactive oxygen species (OH^-, H_2O_2 and O_2^{2-}). Therefore, holes split up water molecules into hydroxyl ions and proton ions. Then dissolved O_2 is converted to superoxide radical anions ($^{\bullet}O^{2-}$), that react with protons to generate $HO_2^{\bullet}$ radicals, which strike electrons to form hydrogen peroxide anions (HO_2^-). Therefore, they react with protons to form H_2O_2 that penetrates the bacterial cell membrane and suppresses the intracellular metabolic pathways of bacteria (Mwankemwa et al., 2017; Tiwari et al., 2017; Modwi et al., 2017).

The CuO doped ZnO composite gives the most potent antibacterial action because of the release of highly active Cu^{2+} ions that are known to have bactericidal activity. The smaller crystallite size leads to more antibacterial effects because it is well-known that Cu^{2+} ions have a lower ionic radius (1.4 Å) than that of Zn^{2+} ions (1.39 Å) (Liau and Huang, 2017).

5. Conclusion

In summary, the CuO nanoparticles and nanocomposite of ZnO/CuO have been fabricated via pulsed laser ablation in liquid. At first, a ZnO thin film with 260 nm thickness is deposited into the surface of metallic copper via spray pyrolysis. To fabricate ZnO/CuO nanocomposite, a Q switched Nd: YAG laser beam (1064 nm, 10 Hz, pulse energy and pulse with 30 mJ and 10 ns) is focused on the surface of the ZnO thin film for 10 min. Then the fabricated samples (CuO nanoparticles and ZnO/CuO nanocomposite) were investigated for their antibacterial activity against several pathogenic microorganisms, including the gram-positive bacterium *S. aureus* subsp. aureus ATCCBAA-977, and the gram-negative bacteria viz. *E. coli* ATCC8739, *K. pneumonia* subsp. pneumoniae, and *P. aeruginosa* ATCC27853. According to the obtained results, the as-fabricated ZnO/CuO nanocomposite demonstrated outstanding antibacterial activity except in the case of *K. pneumoniae* subsp. pneumoniae ATCC700603. Due to the high performance of antibacterial properties of the samples, the ZnO/CuO nanocomposite can be exploited as an effective material for bacteria-free water systems. We expect that our study will aid in the development of innovative semiconductor-based electrical and optical devices with out-

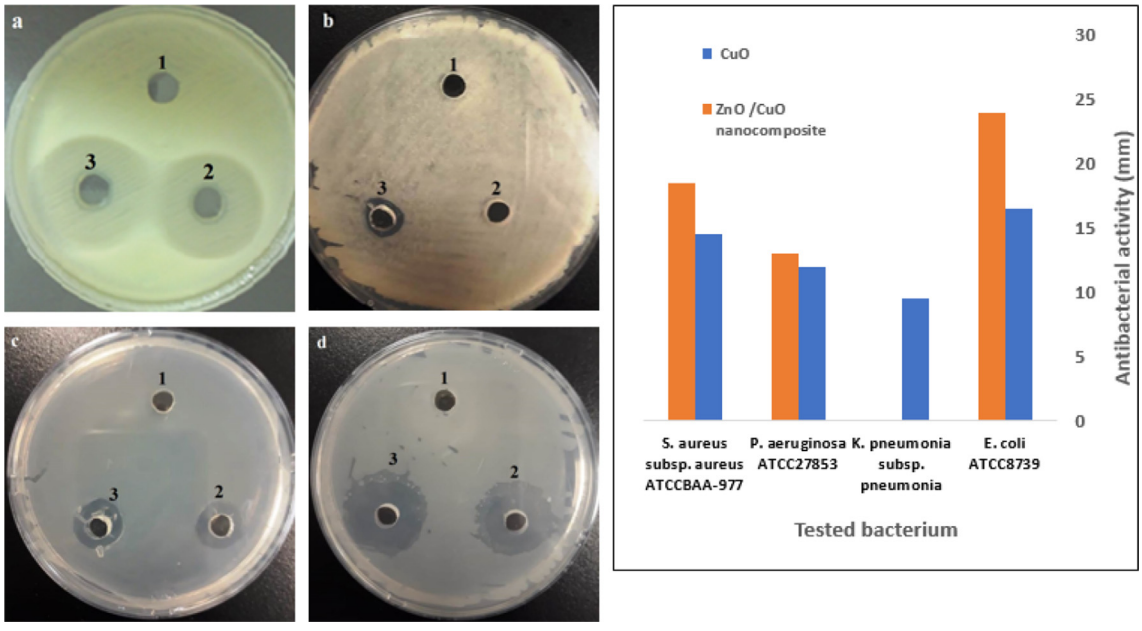

Fig. 7 **(left)** The antibacterial effect of CuO NPs alone (2) and in combination with ZnO NPs **(3)**. Panel (1) corresponds to the control treatment (solvent alone). Panel **(a)** represents *E. coli* ATCC8739 culture, panel **(b)** represents *K. pneumonia* subsp. pneumoniae ATCC700603 culture, panel **(c)** represents *P. aeruginosa* ATCC27853 culture, while panel **(d)** represents *S. aureus* subsp. aureus ATCCBAA-977 culture**.** A bar graph shows the antibacterial activity of CuO and ZnO/CuO nanocomposite against different types of bacteria **(right).**

standing performance, cheap cost, and an efficient manner to open up new opportunities for ZnO/CuO based nanomaterials in the next generation of applications. Furthermore, the discovered synthesis approach may be successfully applied to other nanocomposite oxides.

Declaration of Competing Interest

The authors declare that they have no known competing financial interests or personal relationships that could have appeared to influence the work reported in this paper.

Acknowledgements

Authors extend their appreciation to the Deanship of Scientific Research (DSR), and Deputyship for Research & Innovation, Ministry of Education in Saudi Arabia for funding this research work through the project number 2020-054-CED at Imam Abdulrahman bin Faisal University/College of Education.

References

Iqbal, S., Bahadur, A., Ali, S., Ahmad, Z., Javed, M., Irfan, R.M., Ahmad, N., Qamar, M.A., Liu, G., Akbar, M.B., et al, 2021. Critical Role of the Heterojunction Interface of Silver Decorated ZnO Nanocomposite with Sulfurized Graphitic Carbon Nitride Heterostructure Materials for Photocatalytic Applications. J. Alloys Compd. 858.

Enesca, A., Andronic, L., 2021. Photocatalytic Activity of S-Scheme Heterostructure for Hydrogen Production and Organic Pollutant Removal: A Mini-Review. Nanomaterials.

Kokulnathan, T.; Vishnuraj, R.; Wang, T. J.; Kumar, E. A.; Pullithadathil, B. Heterostructured Bismuth Oxide/hexagonal-Boron Nitride Nanocomposite: A Disposable Electrochemical Sensor for Detection of Flutamide. Ecotoxicol. Environ. Saf. **2021**, 207.

Kokilavani, S., Al-Kheraif, A.A., Thomas, A.M., Syed, A., Elgorban, A.M., Raju, L.L., Das, A., Khan, S.S., 2021. Novel NiS/Ag2MoO4 Heterostructure Nanocomposite: Synthesis, Characterization and Superior Antibacterial and Enhanced Photocatalytic Activity. Phys. E Low-Dimensional Syst. Nanostructures 133.

Sumesh, C.K., 2020. Zinc Oxide Functionalized Molybdenum Disulfide Heterostructures as Efficient Electrocatalysts for Hydrogen Evolution Reaction. Int. J. Hydrogen Energy 45, 619–628.

Wang, B., Cao, J.T., Liu, Y.M., 2020. Recent Progress of Heterostructure-Based Photoelectrodes in Photoelectrochemical Biosensing: A Mini Review. Analyst., 1121–1128

Salehi-Babarsad, F., Derikvand, E., Razaz, M., Yousefi, R., Shirmardi, A., 2020. Heavy Metal Removal by Using ZnO/organic and ZnO/inorganic Nanocomposite Heterostructures. Int. J. Environ. Anal. Chem. 100, 702–719.

Hermawan, A., Zhang, B., Taufik, A., Asakura, Y., Hasegawa, T., Zhu, J., Shi, P., Yin, S., 2020. CuO Nanoparticles/Ti3C2Tx MXene Hybrid Nanocomposites for Detection of Toluene Gas. ACS Appl. Nano Mater. 3, 4755–4766.

Draz, M. A.; El-Maghrabi, H. H.; Soliman, F. S.; Selim, H.; Razik, A. A.; Amin, A. E. sayed; Moustafa, Y. M.; Hamdy, A.; Nada, A. A. Large Scale Hybrid Magnetic ZnFe2O4/TiO2 Nanocomposite with Highly Photocatalytic Activity for Water Splitting. J. Nanoparticle Res. 2021, 23.

Biswal, L., Nayak, S., Parida, K., 2021. Recent Progress on Strategies for the Preparation of 2D/2D MXene/g-C3N4nanocomposites for Photocatalytic Energy and Environmental Applications. Catal. Sci. Technol. 11, 1222–1248.

Mendonça, L.T.B., Bezerra Jr, A.G., de Azevedo, W.M., 2021. Preparation and Caracterization of V2O5 and V2O5/PANI Nanocomposite by Laser Ablation Technique in Liquid. Mater. Chem. Phys. 125084.

Zarschler, K., Rocks, L., Licciardello, N., Boselli, L., Polo, E., Garcia, K.P., De Cola, L., Stephan, H., Dawson, K.A., 2016. Ultrasmall Inorganic Nanoparticles: State-of-the-Art and Perspectives for Biomedical Applications. Nanomed. Nanotechnol. Biol. Med.

Giner-Casares, J.J., Henriksen-Lacey, M., Coronado-Puchau, M., Liz-Marzán, L.M., 2016. Inorganic Nanoparticles for Biomedicine: Where Materials Scientists Meet Medical Research. Mater. Today.

Zhang, X.-L., Zhu, J., Fan, L., Chen, H.-T., Wang, W., He, H., Wang, Q., 2020. Pulsed Laser Ablation in Water Synthesis of Black TiO2-Graphene Oxide Nanocomposites and the Enhanced Photocatalytic Performance. J. Nanosci. Nanotechnol. 20, 2622–2627.

Dhongade, S., Mutadak, P.R., Deore, A.B., More, M.A., Furube, A., Koinkar, P., 2020. In2Se3 Nanocubes as High Current Density Cold Cathode Materials. ACS Appl. Nano Mater. 3, 9749–9758.

Mostafa, A.M., Mwafy, E.A., 2020. The Effect of Laser Fluence for Enhancing the Antibacterial Activity of NiO Nanoparticles by Pulsed Laser Ablation in Liquid Media. Environ. Nanotechnology, Monit. Manag.

Menazea, A. A. Antibacterial Activity of TiO2 Doped ZnO Composite Synthesized via Laser Ablation Route for Antimicrobial Application. J. Mater. Res. Technol. **2020**.

Rishikesan, S., Basha, M.A.M., 2020. Synthesis, Characterization and Evaluation of Antimicrobial, Antioxidant & Anticancer Activities of Copper Doped Zinc Oxide Nanoparticles. Acta Chim. Slov. 67, 235–245.

Alswat, A. A.; Ahmad, M. Bin; Saleh, T. A. Preparation and Characterization of Zeolite\Zinc Oxide-Copper Oxide Nanocomposite: Antibacterial Activities. Colloids Interface Sci. Commun. 2017, 16, 19–24.

Ahamed, M., Alhadlaq, H.A., Khan, M.A.M., Karuppiah, P., Al-Dhabi, N.A., 2014. Synthesis, Characterization, and Antimicrobial Activity of Copper Oxide Nanoparticles. J. Nanomater. 2014.

Mwafy, E.A., Hasanin, M.S., Mostafa, A.M., 2019. Cadmium oxide/TEMPO-Oxidized Cellulose Nanocomposites Produced by Pulsed Laser Ablation in Liquid Environment: Synthesis, Characterization, and Antimicrobial Activity. Opt. Laser Technol. 120.

Mostafa, A.M., Mwafy, E.A., Hasanin, M.S., 2020. One-Pot Synthesis of Nanostructured CdS, CuS, and SnS by Pulsed Laser Ablation in Liquid Environment and Their Antimicrobial Activity. Opt. Laser Technol. 121.

Mostafa, A.M., Mwafy, E.A., 2020. Effect of Dual-Beam Laser Radiation for Synthetic SnO2/Au Nanoalloy for Antibacterial Activity. J. Mol. Struct. 1222.

Khan, M.M., Harunsani, M.H., Tan, A.L., Hojamberdiev, M., Poi, Y. A., Ahmad, N., 2020. Antibacterial Studies of ZnO and Cu-Doped ZnO Nanoparticles Synthesized Using Aqueous Leaf Extract of Stachytarpheta Jamaicensis. Bionanoscience 10, 1037–1048.

Das, S., Srivastava, V.C., 2018. An Overview of the Synthesis of CuO-ZnO Nanocomposite for Environmental and Other Applications. Nanotechnol. Rev., 267–282

Grosso, D.; Boissière, C.; Faustini, M. Thin Film Deposition Techniques. In *The Sol-Gel Handbook*; 2015; Vol. 1-3, pp 277–316.

Perednis, D., Gauckler, L.J., 2005. Thin Film Deposition Using Spray Pyrolysis. J. Electroceramics 14, 103–111.

Filipovic, L., Selberherr, S., Mutinati, G.C., Brunet, E., Steinhauer, S., Kock, A., Teva, J., Kraft, J., Siegert, J., Schrank, F., et al, 2014. Modeling the Growth of Tin Dioxide Using Spray Pyrolysis Deposition for Gas Sensor Applications. IEEE Trans. Semicond. Manuf. 27, 269–277.

Yan, Z., Bao, R., Wright, R.N., Chrisey, D.B., 2010. Hollow Nanoparticle Generation on Laser-Induced Cavitation Bubbles via Bubble Interface Pinning. Appl. Phys. Lett. 97, 24–26.

Bacaksiz, E., Parlak, M., Tomakin, M., Özçelik, A., Karakiz, M., Altunbaş, M., 2008. The Effects of Zinc Nitrate, Zinc Acetate and Zinc Chloride Precursors on Investigation of Structural and Optical Properties of ZnO Thin Films. J. Alloys Compd. 466, 447–450.

Raj Mohamed, J., Amalraj, L., 2016. Effect of Precursor Concentration on Physical Properties of Nebulized Spray Deposited In 2 S 3 Thin Films. J. Asian Ceram. Soc. 4, 357–366.

Althagafi, T.M., Al Baroot, A.F., Grell, M., 2016. A New Precursor Route to Semiconducting Zinc Oxide. IEEE Electron Device Lett. 37, 1299–1302.

Al Baroot, A.F., Grell, M., 2019. Comparing Electron- and Hole Transporting Semiconductors in Ion Sensitive Water- Gated Transistors. Mater. Sci. Semicond. Process. 89, 216–222.

Falcony, C., Aguilar-Frutis, M.A., García-Hipólito, M., 2018. Spray Pyrolysis Technique; High-K Dielectric Films and Luminescent Materials: A Review. Micromachines.

Alheshibri, M., Akhtar, S., Al Baroot, A., Elsayed, K.A., Al Qahtani, H.S., Drmosh, Q.A., 2021. Template-Free Single-Step Preparation of Hollow CoO Nanospheres Using Pulsed Laser Ablation in Liquid Enviroment. Arab. J. Chem. 14, 103317.

Elsayed, K.A., Alomari, M., Drmosh, Q.A., Alheshibri, M., Al Baroot, A., Kayed, T.S., Manda, A.A., Al-Alotaibi, A.L., 2021. Fabrication of ZnO-Ag Bimetallic Nanoparticles by Laser Ablation for Anticancer Activity. Alexandria Eng. J.

Beecher, D.J., Wong, A.C.L., 1994. Identification of Hemolysin BL-Producing Bacillus Cereus Isolates by a Discontinuous Hemolytic Pattern in Blood Agar. Appl. Environ. Microbiol. 60, 1646–1651.

Clinical Laboratory Standards Institute. Methods for Dilution Antimicrobial Susceptibility Tests for Bacteria That Grow Aerobically ; Approved Standard — Ninth Edition. CLSI Document M07-A9. Clin. Lab. Standars Inst. 2018, 32, 18.

Palomino, J.C., Martin, A., Camacho, M., Guerra, H., Swings, J., Portaels, F., 2002. Resazurin Microtiter Assay Plate: Simple and Inexpensive Method for Detection of Drug Resistance in Mycobacterium Tuberculosis. Antimicrob. Agents Chemother. 46, 2720–2722.

Javadpour, M.M., Juban, M.M., Lo, W.C.J., Bishop, S.M., Alberty, J. B., Cowell, S.M., Becker, C.L., De, M.M.L., 1996. Novo Antimicrobial Peptides with Low Mammalian Cell Toxicity. J. Med. Chem. 39, 3107–3113.

Veisi, H., Karmakar, B., Tamoradi, T., Hemmati, S., Hekmati, M., Hamelian, M., 2021. Biosynthesis of CuO Nanoparticles Using Aqueous Extract of Herbal Tea (Stachys Lavandulifolia) Flowers and Evaluation of Its Catalytic Activity. Sci. Rep. 11.

Tiwari, P. K.; Shweta; Singh, A. K.; Singh, V. P.; Prasad, S. M.; Ramawat, N.; Tripathi, D. K.; Chauhan, D. K.; Rai, A. K. Liquid Assisted Pulsed Laser Ablation Synthesized Copper Oxide Nanoparticles (CuO-NPs) and Their Differential Impact on Rice Seedlings. Ecotoxicol. Environ. Saf. 2019, 176, 321–329.

Rawat, R., Tiwari, A., Arun, N., Rao, S.V.S.N., Pathak, A.P., Tripathi, A., 2019. Solvents Effect on the Morphology and Stability of Cu/CuO Nanoparticles Synthesized at High Fluence Laser Ablation. ChemistrySelect 4, 10471–10482.

Gondal, M.A., Drmosh, Q.A., Yamani, Z.H., Saleh, T.A., 2009. Synthesis of ZnO 2 Nanoparticles by Laser Ablation in Liquid and Their Annealing Transformation into ZnO Nanoparticles. Appl. Surf. Sci. 256, 298–304.

Cullity, B.D., 1956. Elements of X-Ray Diffraction. Addison-Wesley Publishing Company, Massachusetts).

Joya, M.R., Barba-Ortega, J., Raba, A.M., 2019. Vibrational Raman Modes and Particle Size Analysis of Cupric Oxide with Calcination Temperature. Indian J. Pure Appl. Phys. 57, 268–271.

Hagemann, H.; Bill, H.; sadowski, W.; Walker, E.; François, M. Raman Spectra of Single Crystal CuO. Solid State Commun. 73 (1990), 447–451.

Prabhu, R.R., Saritha, A.C., Shijeesh, M.R., Jayaraj, M.K., 2017. Fabrication of P-CuO/n-ZnO Heterojunction Diode via Sol-Gel Spin Coating Technique. Mater. Sci. Eng. B Solid-State Mater. Adv. Technol. 220, 82–90.

Bade, B. R.; Rondiya, S. R.; Hase, Y. V.; Nasane, M. P.; Jathar, S. B.; Barma, S. V.; Kore, K. B.; Nilegave, D. S.; Jadkar, S. R.; Funde, A. M. Hydrothermally Synthesized CuO Nanostructures and 7kHLU Application in Humidity Sensing. In *AIP Conference Proceedings*; 2021; Vol. 2335.

Fang, J., Xuan, Y., 2017. Investigation of Optical Absorption and Photothermal Conversion Characteristics of Binary CuO/ZnO Nanofluids. RSC Adv. 7, 56023–56033.

Das, B., Sa, K., Chandra Mahakul, P., Subramanyam, B.V.R.S., Das, S., Alam, I., Raiguru, J., Mahanandia, P., 2018. Efficient Ultraviolet Photodetector Device Based on Modulated Wide Band Gap Type-II CuO/CdSe Core-Shell Nanowires. Superlattices Microstruct. 123, 234–241.

Han, B.; Wu, L.; Li, J.; Wang, X.; Peng, Q.; Wang, N.; Li, X. A Nanoreactor Based on SrTiO3 Coupled TiO2 Nanotubes Confined Au Nanoparticles for Photocatalytic Hydrogen Evolution. Int. J. Hydrogen Energy (**2019**).

Daira, R., Kabir, A., Boudjema, B., Sedrati, C., 2020. Structural and Optical Transmittance Analysis of CuO Thin Films Deposited by the Spray Pyrolysis Method. Solid State Sci. 104.

Dey, K.K., Kumar, A., Shanker, R., Dhawan, A., Wan, M., Yadav, R. R., Srivastava, A.K., 2012. Growth Morphologies, Phase Formation, Optical & Biological Responses of Nanostructures of CuO and Their Application as Cooling Fluid in High Energy Density Devices. RSC Adv. 2, 1387–1403.

Silambarasan, M., Saravanan, S., Soga, T., 2014. Mn-Doped ZnO Nanoparticles Prepared by Solution Combustion Method. In e-Journal Surf. Sci. Nanotechnol. 12, 283–288.

Ibrahim, A., Akhtar, S., Atieh, M., Karnik, R., Laoui, T., 2015. Effects of Annealing on Copper Substrate Surface Morphology and Graphene Growth by Chemical Vapor Deposition. Carbon N. Y. 94, 369–377.

Allahyari, S., Haghighi, M., Ebadi, A., Qavam Saeedi, H., 2014. Direct Synthesis of Dimethyl Ether as a Green Fuel from Syngas over Nanostructured CuO-ZnO-Al2O3/HZSM-5 Catalyst: Influence of Irradiation Time on Nanocatalyst Properties and Catalytic Performance. J. Power Sources 272, 929–939.

Saravanakkumar, D., Sivaranjani, S., Kaviyarasu, K., Ayeshamariam, A., Ravikumar, B., Pandiarajan, S., Veeralakshmi, C., Jayachandran, M., Maaza, M., 2018. Synthesis and Characterization of ZnO-CuO Nanocomposites Powder by Modified Perfume Spray Pyrolysis Method and Its Antimicrobial Investigation. J. Semicond. 39.

Mohammadi-Aloucheh, R., Habibi-Yangjeh, A., Bayrami, A., Latifi-Navid, S., Asadi, A., 2018. Enhanced Anti-Bacterial Activities of ZnO Nanoparticles and ZnO/CuO Nanocomposites Synthesized Using Vaccinium Arctostaphylos L. Fruit Extract. Artif. Cells, Nanomed. Biotechnol. 46, 1200–1209.

Li, H., Chen, Q., Zhao, J., Urmila, K., 2015. Enhancing the Antimicrobial Activity of Natural Extraction Using the Synthetic Ultrasmall Metal Nanoparticles. Sci. Rep. 5.

Mwankemwa, B.S., Legodi, M.J., Mlambo, M., Nel, J.M., Diale, M., 2017. Structural, Morphological, Optical and Electrical Properties of Schottky Diodes Based on CBD Deposited ZnO: Cu Nanorods. Superlattices Microstruct. 107, 163–171.

Tiwari, N., Lohar, A., Kamal, C., Chakrabarti, A., Prajapat, C.L., Mishra, P.K., Mondal, P., Karnar, B., Misra, N.L., Jha, S.N., et al, 2017. Structural and Magnetic Studies on (Fe, Cu) Co-Doped ZnO Nanocrystals. J. Phys. Chem. Solids 104, 198–206.

Modwi, A., Lemine, O.M., Alshammari, M., Houas, A., 2017. Ferromagnetism at Room Temperature in Zn0.95Cu0.05O Nanoparticles Synthesized by Sol-Gel Method. Mater. Lett. 194, 98–101.

Liau, L.C.K., Huang, J.S., 2017. Energy-Level Variations of Cu-Doped ZnO Fabricated through Sol-Gel Processing. J. Alloys Compd. 702, 153–160.